Energy Conversion and Management 284 (2023) 116991

Contents lists available at ScienceDirect

Energy Conversion and Management

journal homepage: www.elsevier.com/locate/enconman

An insight on the physical mechanisms responsible of power augmentation in a pair of counter-rotating Darrieus turbines

Omar S. Mohamed, Pier Francesco Melani, Francesco Balduzzi, Giovanni Ferrara, Alessandro Bianchini *

Department of Industrial Engineering, Università degli Studi di Firenze, Via di Santa Marta 3, 50139 Firenze, Italy

ARTICLE INFO

Keywords:
Darrieus
Vertical Axis Wind Turbines (VAWT)
Hydrokinetic energy
Angle of attack
CFD

ABSTRACT

In recent years, Darrieus turbines have received increasing attention by both the industrial and the academic sector due to their advantages for both wind and hydrokinetic applications. Experimental and numerical investigations showed that the interaction between closely spaced Darrieus rotors can lead to a significant increase in their efficiency. To date, however, the physics underlying this phenomenon has been only argued or qualitatively discussed, since no robust method to determine the actual angle of attack was available.

This study provides a novel insight into the physical mechanisms that lead to performance enhancement in twin Darrieus rotors. A pair of counter-rotating, two-blade Darrieus hydrokinetic turbines are investigated while spinning in both the revolution senses, namely, *inward* and *outward*, by means of unsteady Computational Fluid Dynamics. After a preliminary analysis on the effect of rotor spacing, an improved flow sampling method is used to analyze the instantaneous flow kinematics past the blades in combination with computed blade loads, thus allowing the calculation of lift and drag forces. Results show that the optimum center-to-center distance for the turbines under consideration is 2D. Also, it is shown that the optimum operating point of the twin rotors tends to shift toward higher Tip-Speed Ratios (TSRs). Compared to the stand-alone turbine, the efficiency improves by 16.1% and 8.7% for the *inward* and *outward* twin rotors setups, respectively. A detailed study of the local flow field shows a complete suppression of the streamtube expansion within the area of mutual interactions between the adjacent rotors. This allows more momentum flux to enter the rotor area compared to that of the isolated rotor. More interestingly, it is observed that the change in the inflow velocity direction leads to an increase in the angle of attack for both the *inward* and *outward* setups, causing an increase in the generated lift, which is found as the main reason for the efficiency improvement.

1. Introduction

Research interest in Vertical Axis Wind Turbines (VAWTs) has been increasing significantly during the last couple of decades, targeting different potential applications, from small-scale urban power generation [1] up to large-scale floating offshore installations [2]. These machines are known for the independence of their performance on the wind direction and the low-noise operation. Above all, they come with the unique benefit of having the torque transmitted through a vertical shaft, thus providing the possibility of positioning the powertrain not at height like in their horizontal-axis counterparts. The latter advantage makes the Darrieus turbine economically attractive for some applications such as Floating Offshore Wind Turbines (FOWTs) [3], but also for Hydrokinetic Turbines (HKTs), since in this case the generator can be placed out of the water, with huge benefits in terms of installation, reliability and cost. However, Darrieus turbines are still underperforming in terms of efficiency if compared to horizontal-axis ones [4].

Studies have found that the aero/hydrodynamic efficiency of Darrieus turbines can be improved if two or more rotors are deployed in close proximity, resulting in an increased power generation compared to a standalone turbine [5,6]. This characteristic not only minimizes the efficiency gap between Darrieus and horizontal-axis turbines, but also increases the power density (i.e., power output per occupied land area) of Darrieus turbines. In fact, this concept has attracted the interest of the industrial sector recently in different applications, such as Nenuphar's Twinfloat concept [7], which involves two floating Darrieus wind turbines sharing a common platform, and HE-Powergreen's array [8], which is composed of four hydrokinetic Darrieus turbines sharing the

* Corresponding author.
E-mail address: alessandro.bianchini@unifi.it (A. Bianchini).

https://doi.org/10.1016/j.enconman.2023.116991
Received 16 February 2023; Received in revised form 29 March 2023; Accepted 30 March 2023
Available online 6 April 2023

same supporting structure on a channel. However, a significant drawback of this compact setup is that the performance becomes more sensitive to the inflow direction, depriving the machine of its omnidirectional advantage. In the case of hydrokinetic turbines investigated in this study, characterized by the unidirectional nature of water streams, closely spaced Darrieus turbines could be an optimal solution for power generation.

Dabiri [5] has conducted a campaign of field tests to demonstrate that counter-rotating closely spaced Darrieus turbines produce more power compared to the stand-alone turbine. Vergaerde et al. [6] performed wind tunnel tests for a pair of VAWTs. They concluded an optimum center-to-center spacing of 1.2 and 1.3 rotor diameters, with a relative power increase if 16% compared to an isolated rotor. Li et al. [9] carried out an experimental investigation on the performance of twin Darrieus rotors in an urban environment; they in fact observed an improvement in the performance if the turbines are placed within a closely spaced distance. Müller et al. [10] experimentally analyzed the wake behind twin Darrieus hydrokinetic turbines. They concluded that the slower wake recovery was in the case where the blades are counter-rotating in the inflow direction, while pointing out that the faster wake recovery was in the case of counter-rotating against the inflow direction.

Besides experimental studies, several numerical investigations focused on investigating the optimal spacing and angle that should be kept between two or more Darrieus turbines. Mohamed et al. [11] concluded that closely spaced rotors are more efficient if they are deployed in-line with zero oblique angles. Zheng et al. [12] confirmed the efficient performance of the in-line setup and recommended a spacing distance between 1.5D and 1.6D to maximize the overall cluster efficiency. Sahebzadeh et al. [13] on the other hand studied the co-rotating configuration of a Darrieus turbine pair at different layout arrangements. They found that the co-rotating configuration can reach a maximum overall efficiency almost equal to that of the single rotor. Zhao et al. [14] concluded that adding a flow deflector between counter-rotating turbines could enhance the overall power coefficient by up to 23%. However, it makes the performance even more sensitive to the inflow direction.

Other numerical studies were conducted to understand the physical power augmentation mechanism of the twin Darrieus rotors. Through 2D RANS simulations, Zanforlin et al. [15] speculated that there are two reasons for power enhancement, namely the favorable deviation in absolute wind velocity, and the wake contraction in the downwind path that leads to an increase in the momentum flux available. Alexander et al. [16] extended the latter analysis by observing that the volumetric flow that enters the turbine increases when they are deployed closely due to the blockage effect occurring between the adjacent rotors. They also concluded that the majority of power coefficient enhancement occurs during the mutual interaction zone where the blades are closer to each other, whereas, during other azimuthal positions, the performance might be decreased.

In their study, Guilbot et al. [17] analyzed the performance of twin Darrieus rotors with two blades each. Their investigation focused on the impact of rotor distance and rotation orientation on overall performance. Meanwhile, Peng et al. [18] employed the Taguchi method to examine the influence of airfoil profile, pitch angle, solidity ratio, rotational direction, and spacing between the closely-spaced Darrieus turbines on the optimum Tip Speed Ratio (TSR). Their findings revealed that the solidity ratio has the most significant effect on changing the optimal TSR, which aligns with previous research on single rotors [19]. However, they also noted that the optimum TSR for twin rotors differed from that of a single rotor and tended to increase. Recently, Cacciali et al. [8] proposed an optimization tool to maximize the power output of an in-line array of closely-spaced two-bladed hydrokinetic Darrieus turbines using a Double Multiple Stream Tube (DMST) model incorporated with a confined environment flow field analysis to account for the turbine's fluid dynamic losses, turbulent mixing loss, and channel friction losses, allowing the estimation of backwater propagation.

However, beyond the cited works, to date there is a lack of real quantitative analyses regarding the kinematic behavior of turbines within the mutual interaction region. Most of the works in this area focus on optimizing the overall performance of the turbines, while ignoring the mechanism that leads to such enhancements. In spite of their completeness in terms of flow field analysis, none of previous works analyzed how the interaction between the two turbines actually affects the local inflow on the blades. Indeed, to further develop the concept of closely spaced Darrieus turbines, sufficient knowledge of the variation of the local flow kinematics is needed, which could be beneficial during the rotor design process, e.g., airfoil selection, pitch control, etc. In addition, this information can also be used for the validation and tuning of low- and medium-fidelity tools for the simulation of Darrieus turbines.

This limitation can be mainly attributed to a lack of consensus about the correct procedure to sample the angle of attack (AoA) from a Computational Fluid Dynamics (CFD) simulation. Among the most credited ones, one could indicate the *3-Points* [20], *Trajectory* [21], and LineAverage (*LineAvg*) [22]. Nevertheless, these methods have been originally developed and validated for Horizontal Axis Wind Turbines (HAWTs), with only few examples featured the use of these methods to sample the AoA for VAWTs. Among these, one could cite that of Elsakka et al. [23], where the AoA was sampled on two points upstream of the airfoil. However, the validation for this method was conducted on a static airfoil, which does not encompass the complex phenomena associated with functioning of a Darrieus rotor. Previous works by the authors in Ref. [24,25] compared different methods for sampling the AoA at different operating conditions of the Darrieus turbine, and it has been concluded that the *LineAvg* technique is the most effective among the AoA sampling methods, in terms of data smoothness and reliability. According to these studies, the *Trajectory* shows significant discontinuities near zero AoA, likely because it is an iterative technique and suffers from convergence issues. On the other hand, the *3-Points* or other similar variations (*2-Points* in Ref. [23]) underestimates blade AoA, particularly at low TSRs where flow separation vortices can overlap with one of the sampling points, creating disturbances in the AoA samples. This results in unphysical trends in the computed aerodynamic coefficients.

1.1. Objectives and outline of the study

This paper aims at a more profound physical understanding of the power improvement mechanisms in closely spaced Darrieus rotors, emphasizing the rotors' mutual interactions. This has been achieved by sampling the instantaneous flow velocities near the blade, which are then used to evaluate the amount of momentum flux that enters the rotor domain, quantified via the induction factor (a). AoA data, combined with computed blade forces, were then used to obtain the lift and drag forces on the turbine blade during a full revolution. The element of novelty in this paper is then the quantitative evaluation of how the interaction between two closely spaced Darrieus rotors affects the local blade inflow.

A couple of Darrieus rotors was selected as a study case and analyzed for different spatial arrangements and in the two possible orientations of the counter-rotating configuration, namely, *inward* and *outward*. Different spacings between the rotors were investigated, using only the inline arrangement. Results were then compared with the performance of the stand-alone rotor in terms of blade kinematics, namely the instantaneous angle of attack and torque on a single blade, and the total volumetric flux through the rotor area. Finally, the lift and drag characteristics were evaluated.

The paper is structured as follows. In Section 2, a description of the test case is provided by reporting the geometrical and operational characteristics of the turbine, together with the performance parameters used in the current analysis. In Section 3, the numerical methodology is discussed, describing the geometry and mesh properties as well as the chosen simulation setup. After that, the local flow sampling strategy (*LineAvg*) and its settings are described. Section 4 shows a selection of

main results into two parts. In the first one, the average and instantaneous power outputs for the tested cases are shown, comparing the performance of the counter-rotating turbines with that of the stand-alone one. In the second part, the kinematic characteristics are presented in the form of induction factor, AoA, and chord-based Reynolds number Re_c, followed by an analysis of the lift generation for a single cycle. Finally, conclusions and future work are discussed in Section 5.

2. Test case

2.1. Turbine model

The selected test case is a small-size, two-blade H-Darrieus hydrokinetic turbine designed with an industrial partner by some of the authors in a previous work [26]. This turbine has also been used as a case study for a new active pitch control concept in [27]. In addition, it was one of the turbines used to develop the medium-fidelity simulation tool, the Actuator Line Method (ALM) for Darrieus turbines in [28,29].

An illustration of the turbine geometry is shown in Fig. 1a. It is important to note that only two-dimensional geometry was considered in the present study. Turbine blades are based on a DU-06-W-200 airfoil with a chord length of 0.25 m. Turbine diameter is 2 m. Other geometrical characteristics are reported in Table 1. The optimum operating condition of the isolated rotor corresponding to a Tip-Speed Ratio (TSR) of 2.5 and a power coefficient of approximately 0.38 [26], as shown in Fig. 1b. More details on the operational characteristics are mentioned in Table 2. The twin-rotor configuration was simulated in the counter-rotating setup, taking both rotational orientations into account, i.e., *inward* and *outward* (see Fig. 2). Three spacings were evaluated for each configuration, namely S/D = 1.8, 2, and 2.5.

2.2. Performance parameters

The hydrodynamic performance was quantified using dimensionless parameters, namely, torque coefficient, C_T (Eq. (1)), power coefficient C_P (Eq. (2)), and TSR, λ (Eq. (3)).

$$C_T = \frac{T}{0.5\rho A R V_\infty{}^2} \tag{1}$$

$$C_p = \frac{P}{0.5\rho A V_\infty{}^3} \tag{2}$$

$$\lambda = \frac{\omega R}{V_\infty} \tag{3}$$

Table 1
Geometrical characteristics of the test case turbine.

Dimension	Value
Number of blades [-]	2
Diameter, D [m]	2
Chord, c [m]	0.25
Rotor solidity (Nc/D), σ [-]	0.25
Airfoil	DU06W200
Blade-spoke connection [x/c]	0.25

Table 2
Test operating conditions.

Parameter	Value
Tip-speed ratio [-]	2.5
Rotational speed, ω [rad/s]	5
Work fluid [-]	water
Inflow speed, V_∞ [m/s]	2
Inflow temperature [°C]	25
Inflow turbulence intensity [%]	0.24

In Eqs. (1)–(3), T is the torque on the shaft, ρ is the inflow density, A is the turbine frontal area, R is the radius of the turbine, V_∞ is the inflow velocity, P is the produced hydrodynamic power, and ω is the rotational speed. C_T was computed for each blade individually every timestep and then averaged over a full cycle to calculate the C_P. Although the flow field around the twin rotors is symmetrical, to minimize numerical errors, all performance parameters were averaged across both turbines. For example, (Eq. (4)) shows how the instantaneous global torque coefficient for the twin rotors system was calculated.

$$C_T(\theta) = \frac{C_{T,rotor1}(\theta) - C_{T,rotor2}(\theta)}{2} \tag{4}$$

3. Numerical model

3.1. CFD model

All simulations were conducted using the commercial CFD software ANSYS© FLUENT© version R20.2, using the Unsteady Reynolds-Averaged Navier-Stokes (U-RANS), two-dimensional, pressure-based solver. To minimize numerical diffusion errors, the second-order upwind convection scheme was utilized for the approximation of the convection/diffusion terms. An angular timestep $\Delta\theta$ of 0.4° was used for all simulations with the second-order implicit time advancing scheme.

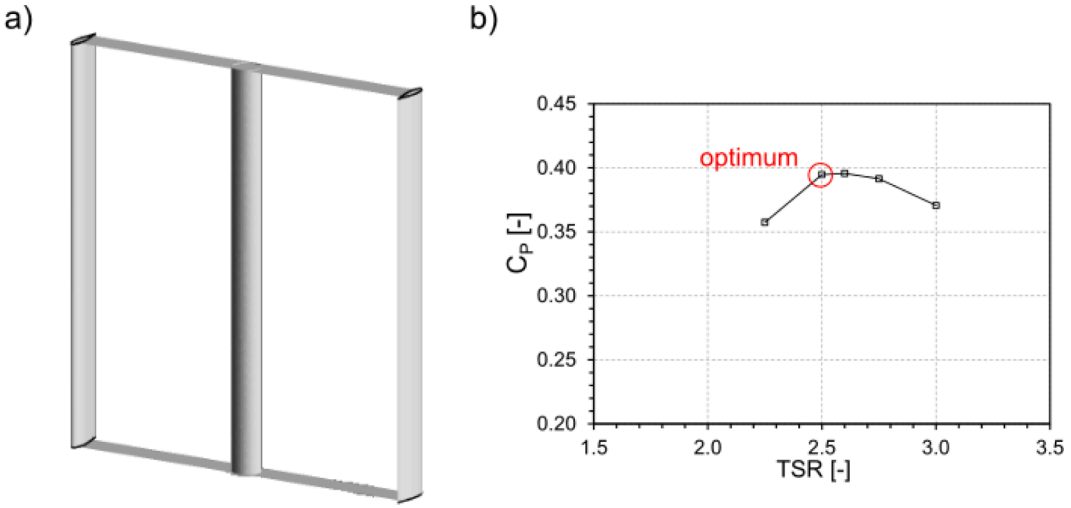

Fig. 1. A) schematic representation of the reference turbine and b) the performance curve.

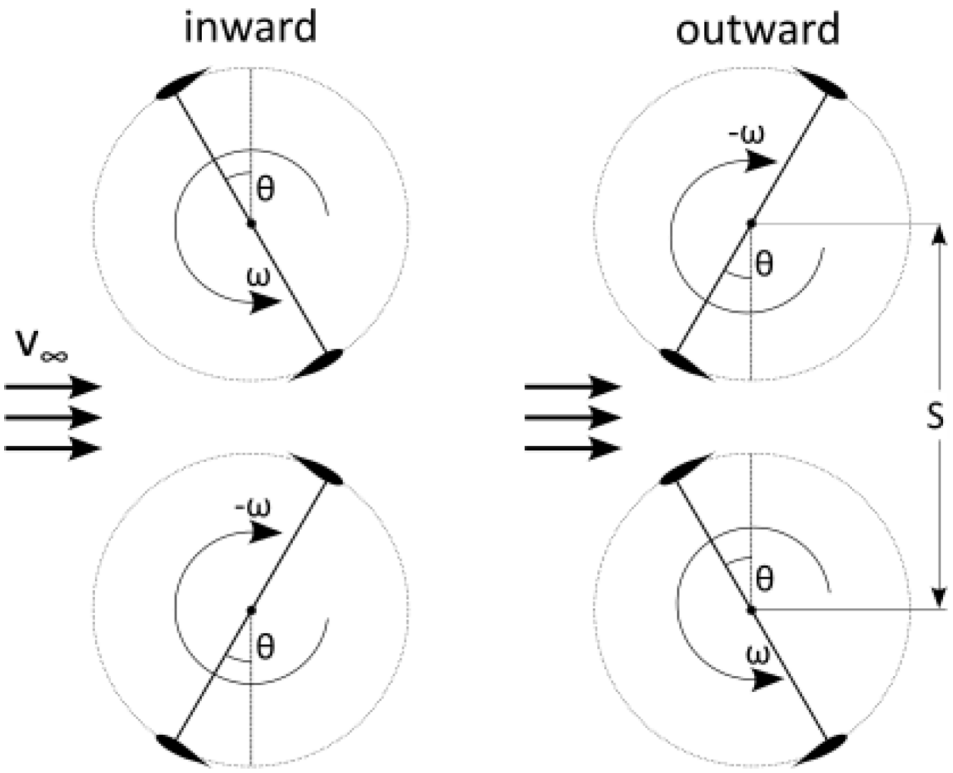

Fig. 2. Schematic representation of the inward (left) and outward (right) configurations.

The solution periodic convergence was assessed based on the average torque for a complete revolution. A threshold of 0.1% residual in the average torque was adopted, corresponding in approximately 25 revolutions depending on the operating point. Thus, only results of the last cycle were considered. The *k-ω SST* turbulence model [30] was used for turbulence closure.

The choice of the numerical schemes and turbulence model was based on the experience of the authors on similar test cases [31,32]. The temporal and spatial discretization levels were selected to be in line with the comprehensive sensitivity studies conducted by the authors in [31,33], and particularly to be compliant with the dimensionless vorticity and Courant number thresholds proposed in [34]. The size of the computational domain size was adopted from previous studies on a single rotor [31], with some adjustments to accommodate the blockage

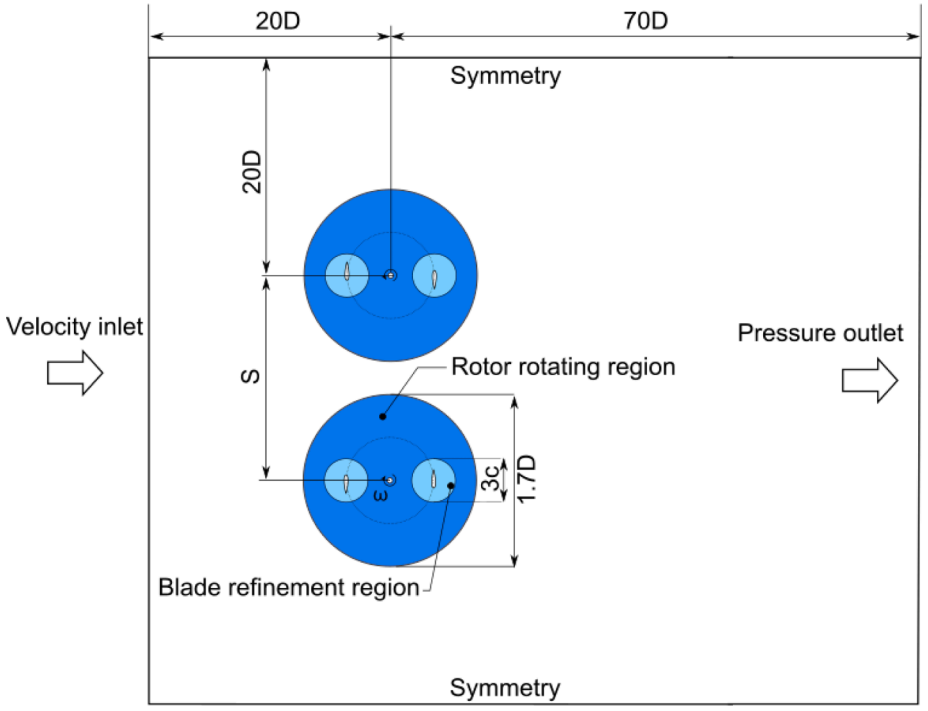

Fig. 3. Computational domain schematic.

effect due to the presence of two rotors. The domain was enlarged in the crosswise direction by a length *S*, which is the distance between the rotors. The domain consists of two rotating zones and a stationary zone. The rotating sub-domains and the stationary sub-domain were separated using non-conformal mesh where the *sliding mesh* technique was applied. The rotating domain was designed to be 1.7D. The details of the domain dimensions as well as the boundary conditions are shown in Fig. 3.

Regarding the mesh, a non-structured mesh was adopted, similar to that applied in previous works of [31,33]. In this grid, the finest mesh was created in the zones surrounding the airfoils, using prismatic elements near the walls as shown in Fig. 4e. As required for the k-ω SST turbulence model, the first cell layer from the wall was sized to reach a dimensionless wall distance $y^+ < 1$. The rotating domains were divided into sections to ensure a gradual transition from the fine elements near the airfoil up to the coarse elements in the stationary domain. For the latter, two wake zones were created, where the mesh density increases gradually from the twin rotors until reaching the far field. The total element size of the created mesh is ≈ 1,500 k. Table 3 reports the features of the mesh and Fig. 3 shows the details of the mesh created for the turbine pair.

Table 3
Details of the adopted mesh.

Parameter	Value
# elements in stationary domain	526,712
# elements in each rotating domain	490,136
# nodes on the blade	1440
# inflation layers on the airfoil	60

3.2. Angle of attack sampling

Darrieus turbines are characterized by their complex flow field and unsteadiness as illustrated in Fig. 5. During their operation, the blades rotate with a cycloidal motion, causing intrinsic azimuthal variations of the aero/hydrodynamics, which result in complex flow phenomena such as dynamic stall, vortex shedding, and blade-wake interactions [35]. In addition, due to the blockage effect caused by the rotating blades, the inflow that approaches the Darrieus rotor deviates, and forms what is known as streamtube expansion. Hence, a simplified aerodynamic analysis could not achieve accurate estimations of the azimuthal variation of the kinematic quantities, e.g., angle of attack and blade local velocity.

The *LineAverage* method (LineAvg) was used to sample the local velocity field. This technique was first introduced for Horizontal-Axis Wind Turbines (HAWTs) to include the influence of the shedding and the trailing vorticity in the computed AoA [22]. Recently, it has been adapted for Darrieus turbines and validated against blade-resolved CFD and experimental measurements in [24,25]. In these works, it has been shown that the results computed by *LineAvg* could produce some discontinuities at low TSRs due to the interaction between the separation vortices and the sampling line downstream of the airfoil. In the present case, this is not an issue, given the stable operating conditions of the selected twin rotors.

In the *LineAvg*, the undistributed inflow velocity is sampled as an integral average along a closed line around the airfoil, centered in its aerodynamic center, i.e., approximately at 25% of the chord. In this way, the induced velocity components are levelled out during the averaging process, filtering out the effect of the profile bound circulation. Once the local velocities in the x- and y-direction have been sampled, they are combined to calculate the local inflow velocity, $V_{\infty,L}$, which is then combined with the rotor speed, ωR, to compute the AoA and relative velocity V_R:

$$V_{\infty,L} = \sqrt{V_x^2 + V_y^2} \tag{5}$$

$$\alpha = \tan^{-1}\left(\frac{-V_x\sin\theta + V_y\cos\theta}{-V_x\cos\theta - V_y\sin\theta - \omega R}\right) \tag{6}$$

$$V_R = \sqrt{\left(-V_x\sin\theta + V_y\cos\theta\right)^2 + \left(-V_x\cos\theta - V_y\sin\theta - \omega R\right)^2} \tag{7}$$

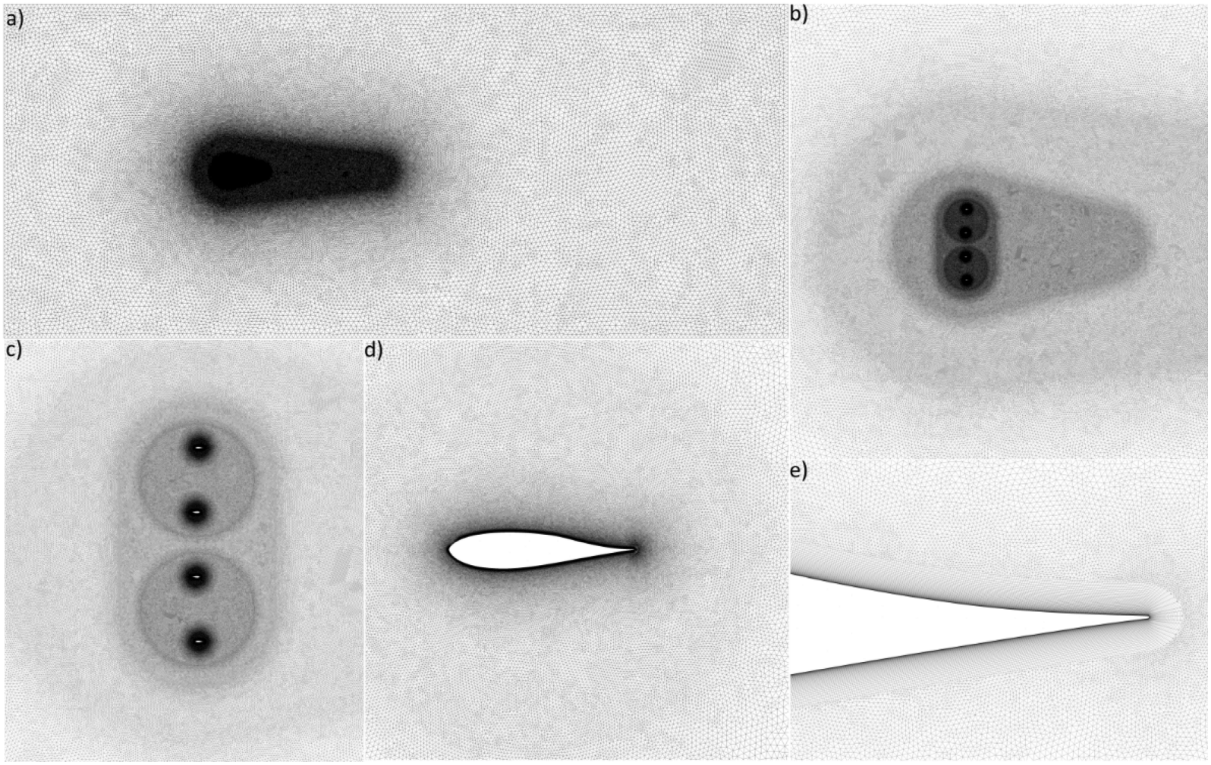

Fig. 4. Details of the adopted mesh: a) far field, b) near wake, c) rotating zones, d) blade, and e) trailing edge.

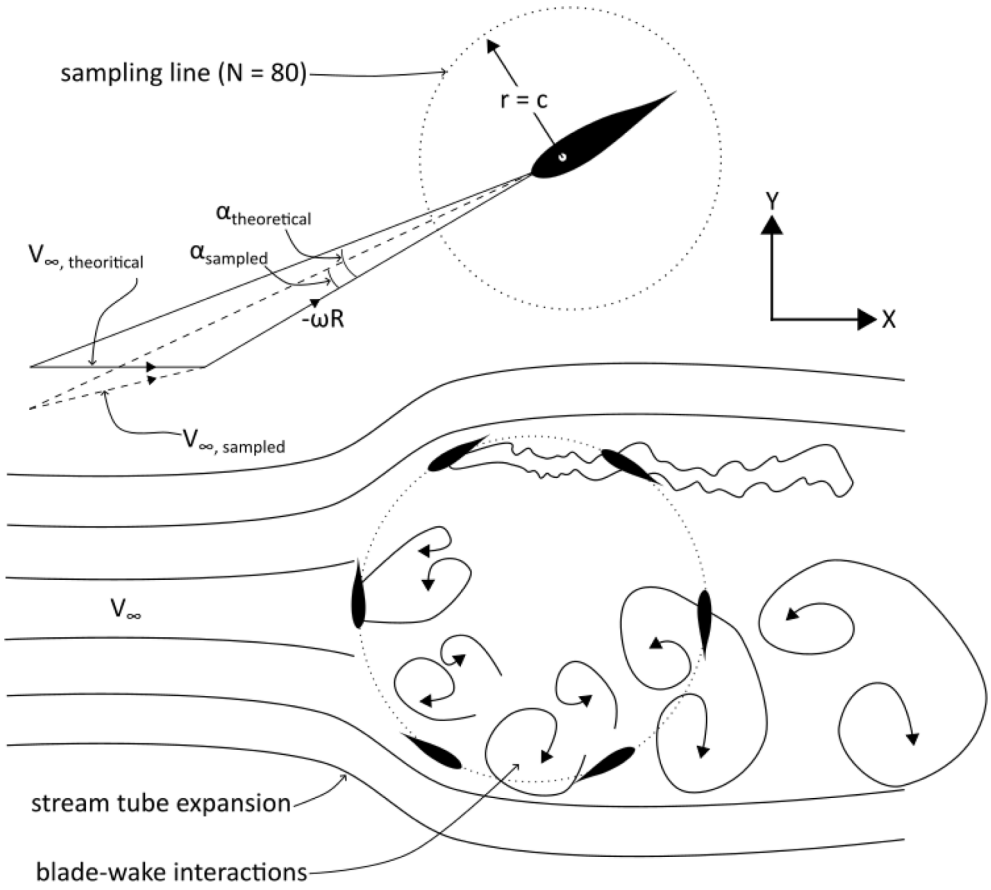

Fig. 5. Schematic representation of the Darrieus rotor flow field and the LinAvg AoA sampling method.

Being able to sample the local flow field, an induction factor (a) equivalent to that of the ubiquitous Blade Element Momentum Theory can be computed to represent the relative decrease in the inflow velocity between the freestream and the rotor domain:

$$a = \frac{V_{\infty} - V_{\infty,L}}{V_{\infty}} \tag{8}$$

In this study, a circular sampling line has been used, with a radius r = 1c and 80 evenly distributed sampling points (see Fig. 5).

4. Results

In this section, the main findings of the current study are presented. First, the performance of the counter-rotating twin rotors is shown at different spacing distances, *S*, for both *inward* and *outward* configurations (S = 1.8D, 2D, and 2.5D), followed by a demonstration of the instantaneous torque production for a full revolution and local blade kinematic analysis. A series of comparisons in terms of angle of attack and induction factor between the single rotor and both configurations of the twin rotors are then presented to understand the flow regime that characterizes the twin rotors. Finally, coupling the kinematic data with its corresponding computed forces allowed the computation of the lift and drag data, which gave an insight into the physical mechanism that leads to an efficiency increase for twin Darrieus rotors.

4.1. Twin rotors performance

Fig. 6 shows the average C_P calculated for each setup at TSR 2.5, compared with that of the single rotor. The efficiency improvement percentage for the twin rotors with respect to the single rotor was calculated as in Eq. (8):

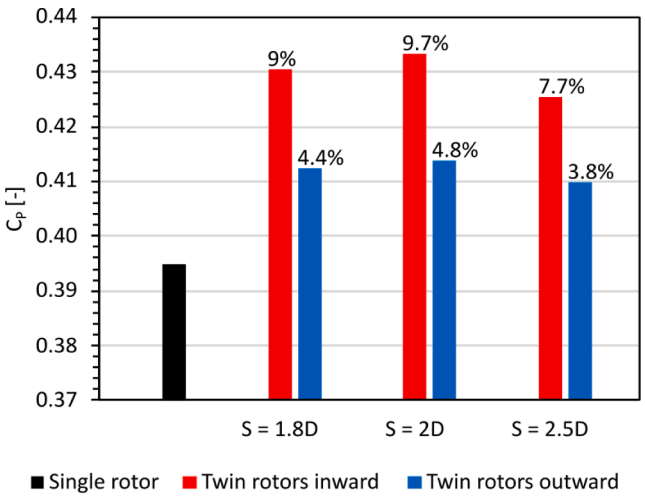

Fig. 6. Average power coefficient at TSR = 2.5 resulted from the twin rotors and their percentage increase compared to single rotor at different separating distances.

$$Performanceincrease[\%] = \frac{C_{P\,TwinRotors} - C_{P\,SingleRotor}}{C_{P\,SingleRotor}} \tag{9}$$

The results show that the separating distance of S = 2D allowed achieving the highest power coefficient for both the *inward* and the *outward* setups, with efficiency improvement of 9.7% and 4.8%, respectively. Thus, this separating distance was considered for further investigations to analyze the mechanisms underlying such performance

enhancement.

To see the influence of TSR on the twin rotors performance, both *inward* and *outward* configurations were tested at different TSRs as reported in Fig. 7 along with the percentage improvement for each case. The results show that the optimum TSR for the twin rotors tends to shift to higher values compared to that of the single rotor, and the efficiency improvement increases with the increase in TSR. The *inward* setup achieves the highest power coefficient of 0.46 at TSR = 3, while the maximum power coefficient *outward* was 0.43 at TSR = 2.75, with percentages improvement of 21.8% and 12.8%, respectively. In general, comparing the optimum operating conditions of the twin rotors with that of the single rotor, the power coefficient improved by 16.1% and 8.7% for the *inward* and *outward*, respectively.

Fig. 8 shows the instantaneous torque coefficient and dimensionless normalized force computed for a single blade for the *inward* and *outward* twin rotors configurations compared with that of the single rotor at TSRs 2.5 and 3, respectively. The quadrant contribution was calculated by integrating the torque within the quarter and then dividing it over the total integral torque. The relative quadrant torque increase or decrease between the twin rotors and the single rotor was computed by multiplying the quadrant contribution by the quadrant percentage improvement. Table 4 reports the percentage power contribution for the single rotor and the rotor pairs with their relative increase/decrease of the twin rotors with respect to the single rotor.

For the *inward* configuration, which achieved higher power enhancements for both TSRs 2.5 and 3, the torque coefficient within the azimuth range of $0^\circ \leq \theta \leq 90^\circ$ is almost the same as that of the single rotor blade, showing a noticeable decrease in the quadrant contribution due to the overall increase in the torque production. The second and third azimuthal quarters, from azimuthal positions from $\theta = 90^\circ$ to $\theta = 270^\circ$ represent the area of mutual interaction, where the blades of the twin rotors are in the closest positions to the adjacent rotor. During the second quarter, almost at all azimuthal positions, the torque coefficient of the twin rotors is higher than that of the single rotor. Indeed, most of the performance enhancement is been achieved during this quarter, having a quadrant contribution of 63% at TSR = 2.5 and 90% at TSR = 3, compared to 60% and 85%, respectively, for the single rotor. The third quarter has a torque generation close to that of the single rotor, with a slight increase which could be better noted at TSR = 2.5 around $\theta \approx 225^\circ$. The final quarter shows almost the same performance as that of the single rotor for both TSRs 2.5 and 3.

Regarding the *outward* configuration, the areas of mutual interaction are the first and fourth quarters, i.e., $0^\circ \leq \theta \leq 90^\circ$ and $270^\circ \leq \theta \leq 360^\circ$.

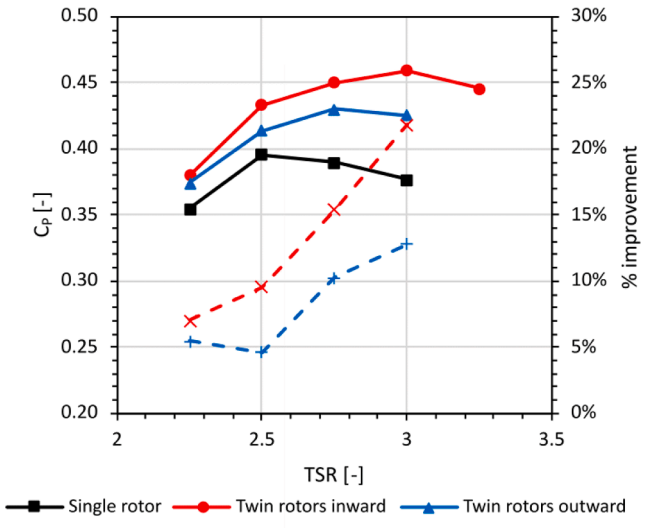

Fig. 7. Average power coefficient against TSR resulted from the twin rotors and their percentage increase compared to single rotor.

In the first quarter, most of the performance enhancement can be observed for both TSRs 2.5 and 3, with a peak torque slightly higher than that of the single rotor. On the other hand, during the second quarter, a small reduction in toque could be noticed at TSR = 2.5, while a slight increase is observed at TSR = 3. From $\theta = 180^\circ$ until $\theta = 360^\circ$ at both TSRs, the performance of the twin rotors is almost equal to that of the single rotor with a slight decrease in the torque coefficient at the last quadrant.

Overall, despite the higher performance enhancement achieved at TSR = 3 compared to that at TSR = 2.5, one can notice the resemblance in the quadrant increase/decrease in torque with respect the single rotor, where the differences are mainly attributed to the influence of the TSR on quadrant torque contribution. It can be observed that for the *inward* setup, most of the enhancements occur during the second quarter, while they occur in the first quadrant for the *outward* setup.

4.2. Induction factor

Although the concept of "induction factor" comes from the one-dimensional momentum theory, it provides an intuitive way to analyze the flow modification and can be then used in a comparative sense to represent the relative decrease of the inflow speed through the turbine area and thus, an indication of the momentum flux that enters the rotor domain. Fig. 9 shows the variation of a of a single blade of the twin rotors compared to that of the single rotor for a full revolution at TSRs 2.5 and 3, respectively. The percentage increase/decrease was also calculated instantaneously and averaged for each azimuthal quarter. As can be seen for both TSRs, for the *inward* configuration, a was close to that of the single rotor during the first quarter, i.e., $0^\circ \leq \theta \leq 90^\circ$, with a decrease of 1.5% and 3.1%, for TSRs 2.5 and 3, respectively. Almost half of the second quarter, from $\theta \approx 90^\circ$ to $\theta \approx 135^\circ$, the induction factor was almost equal for both twin and single rotors. After that, a significant decrease a could be noticed for the *inward* twin rotors until matching again with the single rotor at $\theta \approx 315^\circ$. At TSR = 2.5, during the second and third quarters, a decreased by 3.2% and 7.6%, respectively. Closer reduction in a could also be seen at TSR = 3 with percentages of 3.8% in the second quarter and 6% in the third quarter. At both TSRs, no significant changes occur during the last quarter.

In the case of the *outward* setup, the decrease in a can only be observed in the second and last quarters for both TSRs with 2.4% and 2.5%, respectively, at TSR = 2.5, and 3.4% for both quarters at TSR = 3. Overall, with respect to the single rotor, the induction factor for the *outward* setup decreased by 2% at TSR = 2.5 and 6.9% at TSR = 3. On the other hand, for the *inward* setup it is decreased by 12.5% at TSR 2.5 and 13.6% at TSR = 3.

An interesting point is that the areas with an overall decrease in the induction factor do not always correspond to an increase in power coefficient (see Table 4). In the first quarter of the *inward* setup, the efficiency decreased, and yet the induction factor decreases. Conversely in the outward setup, the quarters where the enhancement of the power coefficient occurs are the same quarters showing an increase in the induction factor, and vice versa. The latter observation confirms that the efficiency improvement of the closely spaced rotors is not directly related to the increased volumetric flux through the rotor as suggested by Alexander et al. [16].

4.3. Blade hydrodynamics

Fig. 9 reports the changes in cyclic AoA (a) and local Reynolds number (b), Re_c, as well as the lift coefficient (c), C_L, for the *inward* and *outward* twin rotors compared to the standalone rotor. The data is shown for TSRs 2.5 and 3, along with the static polar data acquired using XFoil [31]. It is important to note that the static airfoil data presented was obtained for the virtually cambered DU06W200 profile to account for the blade cycloidal motion [37].

At both TSRs, for the *inward* configuration, during the first quarter,

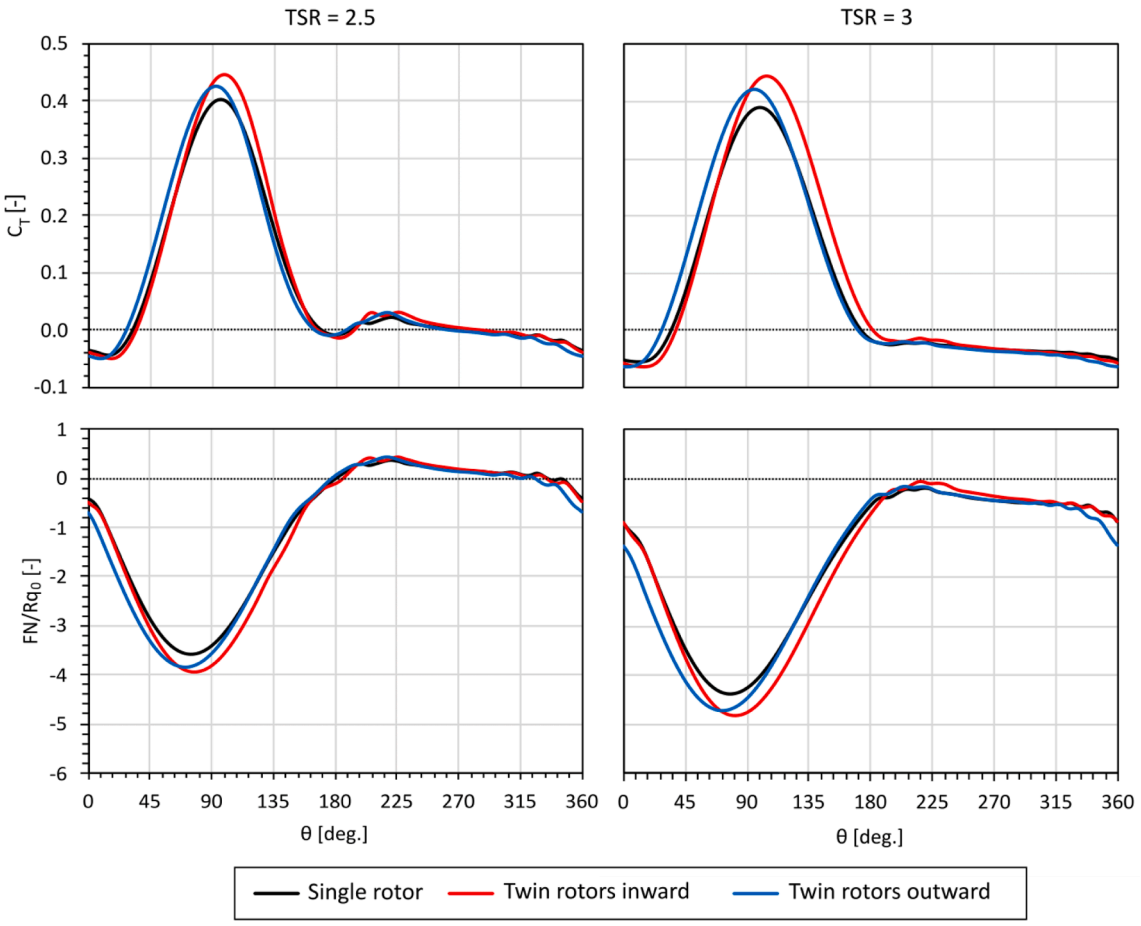

Fig. 8. Instantaneous torque coefficient and normalized normal force computed from the twin rotors at S = 2D and TSRs 2.5 and 3 for inward and outward configurations compared to that of the single rotor.

Table 4
Power contribution for each cycle quarter and the corresponding twin rotors relative improvement/degradation.

θ	Single Rotor	Inward	Outward
		(% increase/decrease)	
TSR = 2.5			
0° to 90°	40.0%	34.7% (−1.7%)	47.3% (11.3%)
90° to 180°	60.1%	63.2% (9.6%)	53.8% (−3.5%)
180° to 270°	3.0%	4.7% (3.3%)	3.6% (0.9%)
270° to 360°	−3.1%	−2.6% (0.2%)	−4.7% (−2.7%)
TSR = 3			
0° to 90°	41.3%	31.7% (−2.0%)	50.3% (18.8%)
90° to 180°	85.2%	89.7% (25.5%)	76.5% (1.0%)
180° to 270°	−10.6%	−7.2% (1.2%)	−10.0% (−0.6%)
270° to 360°	−15.9%	−14.3% (−1.4%)	−16.8% (−3.3%)

the AoA variation matches that of the isolated rotor, the same observation can be made also for Re_c. After that, within the mutual interaction zone ($90° \leq \theta \leq 270°$), the blade experiences significant increases in AoA until $\theta = 180°$, where AoA = 0°, showing a complete suppression of the stream tube expansion effect. Thereafter, the AoA increases again above that of the single rotor after $\theta = 200°$, until $\theta \approx 270°$. Further observation within the mutual interaction zone is that Re_c, after matching with that of the single rotor until $\theta \approx 160°$, decreases significantly up to $\theta \approx 270°$. In the fourth quarter, i.e., $270° \leq \theta \leq 360°$, there are no relevant differences between the twin and isolated rotor.

For the *outward* configuration, in the first quarter, i.e., $0° \leq \theta \leq 90°$, which is a zone of mutual interaction in this setup, the AoA increases slightly compared to the single rotor, while Re_c decreases. The decrease in the Re_c continued until $\theta \approx 160°$, where it matches the single rotor values. Given that the flow in this setup is against the blade direction within the mutual interaction area, the increase in AoA is not as much as in the *inward* configuration. From $\theta \approx 90°$ up to $\theta \approx 330°$, the AoA experienced by the blade of the twin rotors almost matches that of the isolated rotor. Thereafter, it decreases marginally.

The computed lift coefficient displays clear hysteretic behavior, especially at TSR = 2.5, which is typical for Darrieus turbines due to dynamic effects, in particular dynamic stall. During the *pitch-up* phase, both twin rotor setups show slopes comparable to that of the single rotor, albeit with a slight offset towards higher lift values. This offset is more evident when compared to the static lift. As the blade AoA increases from 0° to ≈ −17°, the lift coefficient still increases despite the AoA exceeding the static stall limit. Both twin configurations are characterized by a maximum C_L value ≈ 9% higher than that of the isolated rotor, in particular the *inward* one, which is then penalized afterwards. During the *pitch-down* phase in fact, there is a higher degree of fluctuation in lift variation against the AoA for the different configurations. These variations can be attributed to the AoA fluctuations between $\theta \approx 120°$ and $\theta \approx 225°$, which are related to the mutual interactions between the adjacent rotors. At TSR = 3, this effect is not present anymore, and all rotor configurations show higher lift in comparison to the static coefficients. The dynamic variation of lift at this TSR during the *pitch-down* phase in fact cannot be attributed to dynamic stall, but rather to other unsteady effects associated with elevated reduced frequencies, causing a delay in the effective AoA with respect to the one expected at the given azimuthal position. This phenomenon has been extensively analyzed on results obtained using the *LinAvg* for a Darrieus turbine in Ref. [24].

To see the kinematic characteristics of the twin Darrieus rotors from

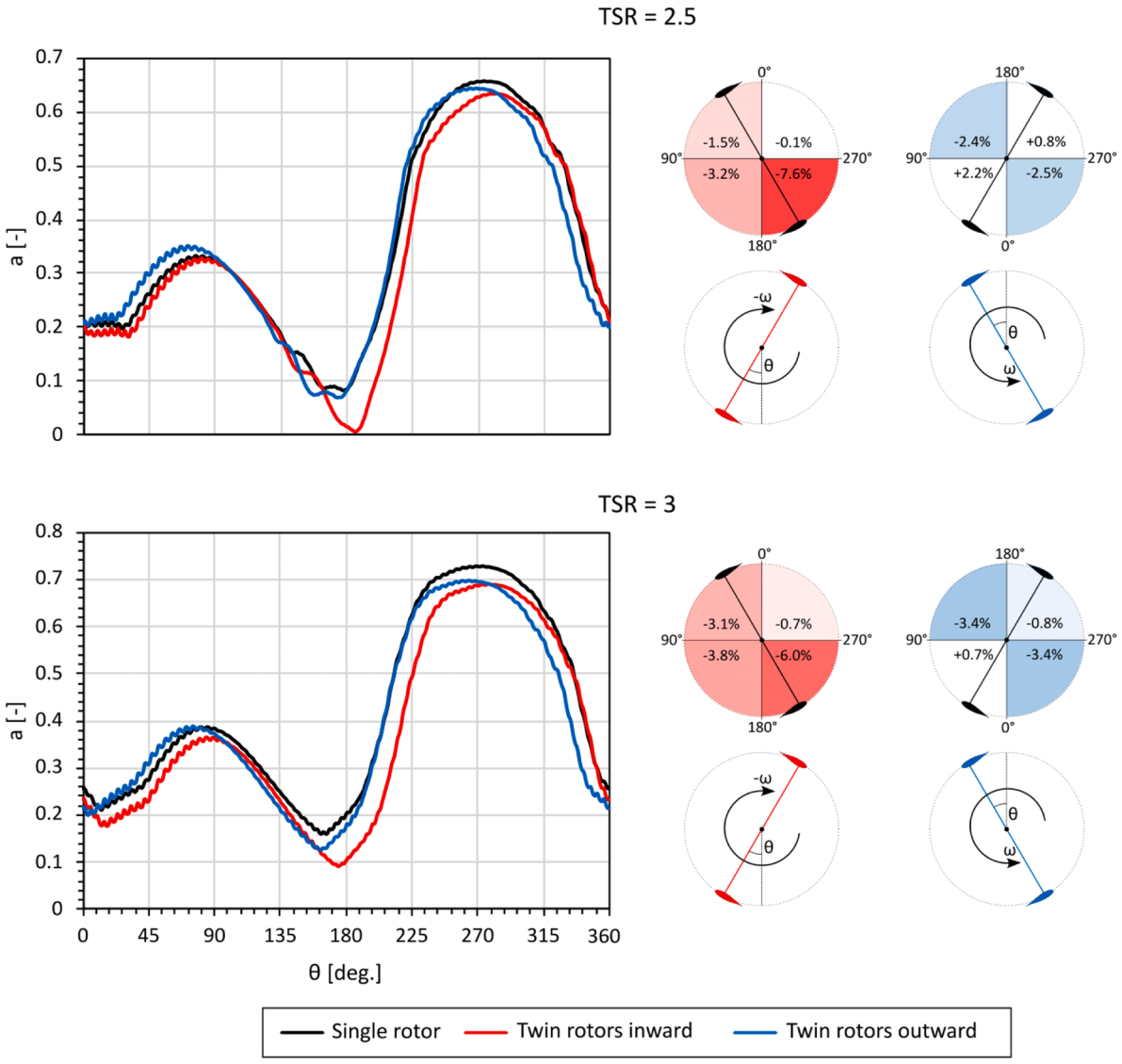

Fig. 9. Cyclic change in the induction factor for the a) inward and b) outward setups at S = 2D compared to that of the single rotor.

a different perspective, Fig. 11 shows the contours of the dimensionless vorticity as well as the streamlines for both the twin rotors configurations and the single isolated rotor at TSR = 3. Upon examination of the streamlines, one can clearly notice the streamtube expansion in the isolated rotor. However, for both the *inward* and *outward* pairs, the mutual interaction between the rotors eliminates the deviation in inflow as marked in the black rectangle. For both cases, the blockage caused by the rotors allows the flow to be constrained in a narrow area, which leads to the suppression of the y-velocity components, making the flow almost straight. It is speculated that the latter effect is the main reason for the AoA increase observed previously (see Fig. 10).

Fig. 12 reports the computed lift coefficient against the azimuth position for both *inward* and *outward* configurations compared with that of the single rotor at TSRs 2.5 and 3. The percentage increase of lift generation for each quarter was calculated as

$$\%C_L increase = \frac{\int \left(|C_L|_{TwinRotors} - |C_L|_{SingleRotor} \right) d\theta}{\int |C_L|_{SingleRotor} d\theta} \quad (10)$$

The percentage increase of C_L for each quarter is close for both evaluated TSRs. For the *inward* configuration, the extra lift generation starts early at $\theta \approx 60^\circ$, it peaks at $\theta \approx 120^\circ$, and then decreases to match with that of the single rotor before the second rise at $\theta \approx 200^\circ$ until matching again with the single rotor during the fourth azimuthal quarter. On the other hand, the *outward* starts with a lift coefficient higher than that of the single rotor until peaking at $\theta \approx 120^\circ$ and then matching with the single rotor up to the fourth quarter, where the blades enter again the zone of mutual interaction, and the lift coefficient starts to be higher than that of the single rotor from $\theta \approx 315^\circ$. For the *inward* setup, the highest percentage increase in lift occurs in the second and third quarters, while for the *outward* setup, it can only be found in the first quarter. Those quarters are also the same quarters with highest relative power coefficient enhancement (see Table 4).

4.4. Effect of azimuth shift

Given that the analyses presented in this work only consider twin rotors with blades perfectly aligned at the same corresponding azimuth positions, which is an ideal case that is hard to achieve in reality, an assessment has been conducted to evaluate the influence of azimuth shift between the two twin rotors, referred to as $\Delta\theta$. Fig. 13 shows the instantaneous azimuthal variation of torque coefficient for the inward setup at TSR = 3 for a perfectly aligned setup, i.e., $\Delta\theta = 0^\circ$ compared with that of $\Delta\theta = 90^\circ$. The choice of the latter azimuth shift is justified as it would be the widest azimuth shift that could be made for two-bladed Darrieus rotors. As can be seen, the torque coefficients of both cases

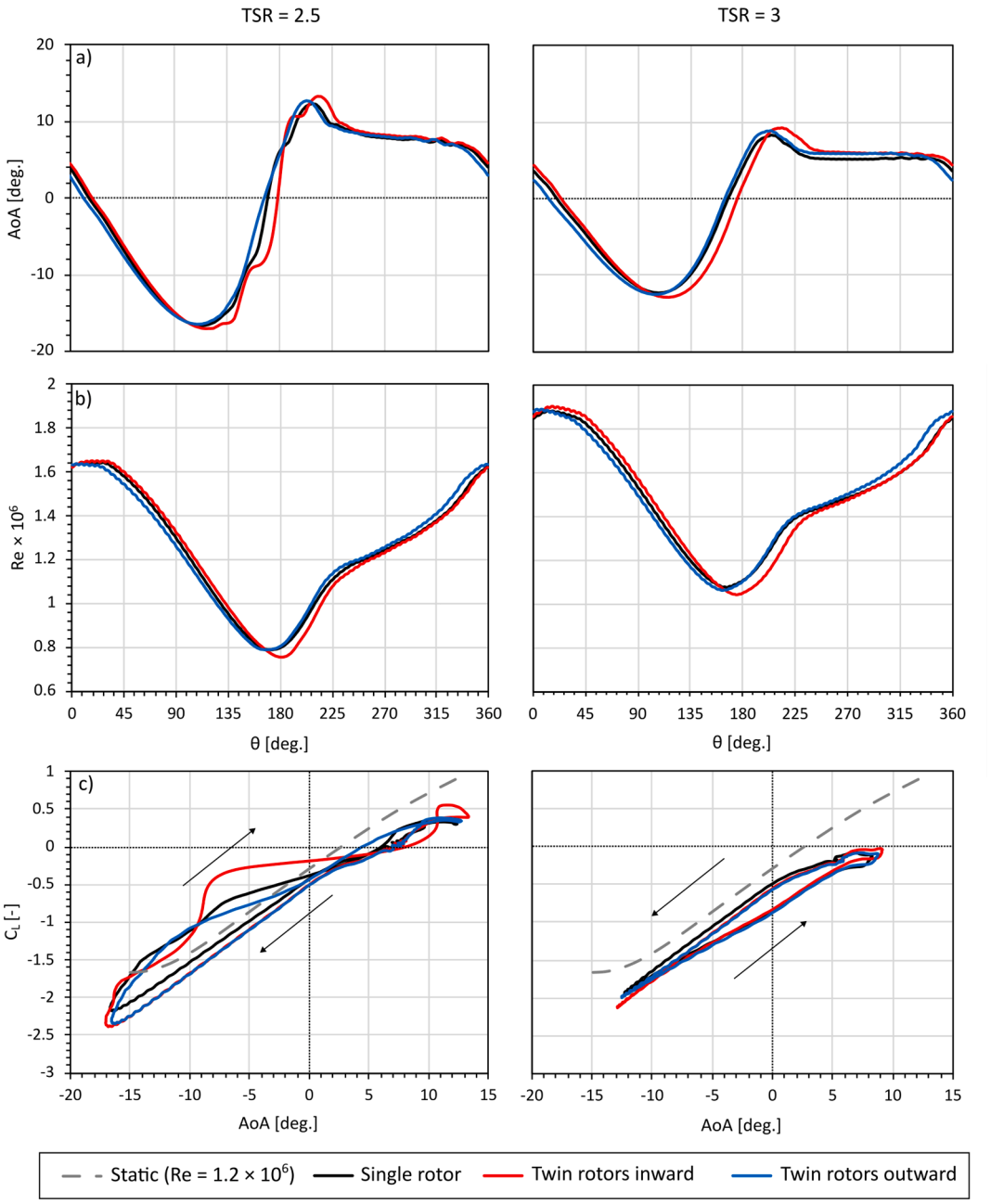

Fig. 10. Cyclic a) AoA and b) Re_c variations against azimuth position, and c) lift hysteresis loop for inward and outward twin rotors at TSRs 2.5 and 3 compared with the single rotor and the static lift.

perfectly match, which agrees with the findings of Jin et al. [36]. Accordingly, from the physical point of view, one can say that the twin rotors are seen by the flow field as spinning closed bodies regardless of the position of the blades, making the effect that the closely spaced rotors are imposing on the approaching flow field, which has been proven to be the main reason of the performance enhancement, uninfluenced by azimuth shift between the turbines.

5. Discussion

The present study quantitatively demonstrates how the efficiency of two closely-spaced counter-rotating Darrieus rotors increases compared to a single rotor. All results were obtained using a two-dimensional CFD U-RANS approach, which has been extensively validated for such an application against experimental results [39,40], and higher-fidelity approaches [41]. CFD settings have been optimized according to more credited best practices for Darrieus turbines [31,42]. However, it is undisputed that this approach might suffer from some limitations, such as overestimating the power coefficient, as tip losses are not considered [43]. Additionally, the real blockage effect given by the two rotors will probably be lower than in 2D, as the flow can partially bypass the turbine in the blade span-wise direction. Therefore, the percentage increase in the power coefficient might actually be lower, as pointed out by Nazari et al. [44]. Complex flow structures and turbulence might be also not completely captured by a RANS approach. However, based on the discussed previous validations of this method and bearing in mind that the effects under investigation are related to the main flow behavior across the turbines, it is reasonable to assume that the results obtained in this study using U-RANS provide a consistent insight into the augmentation mechanism of twin rotors. Moreover, it should be also noted that a comparative approach has been adopted between the configurations, thus reducing the potential impact of some specific settings.

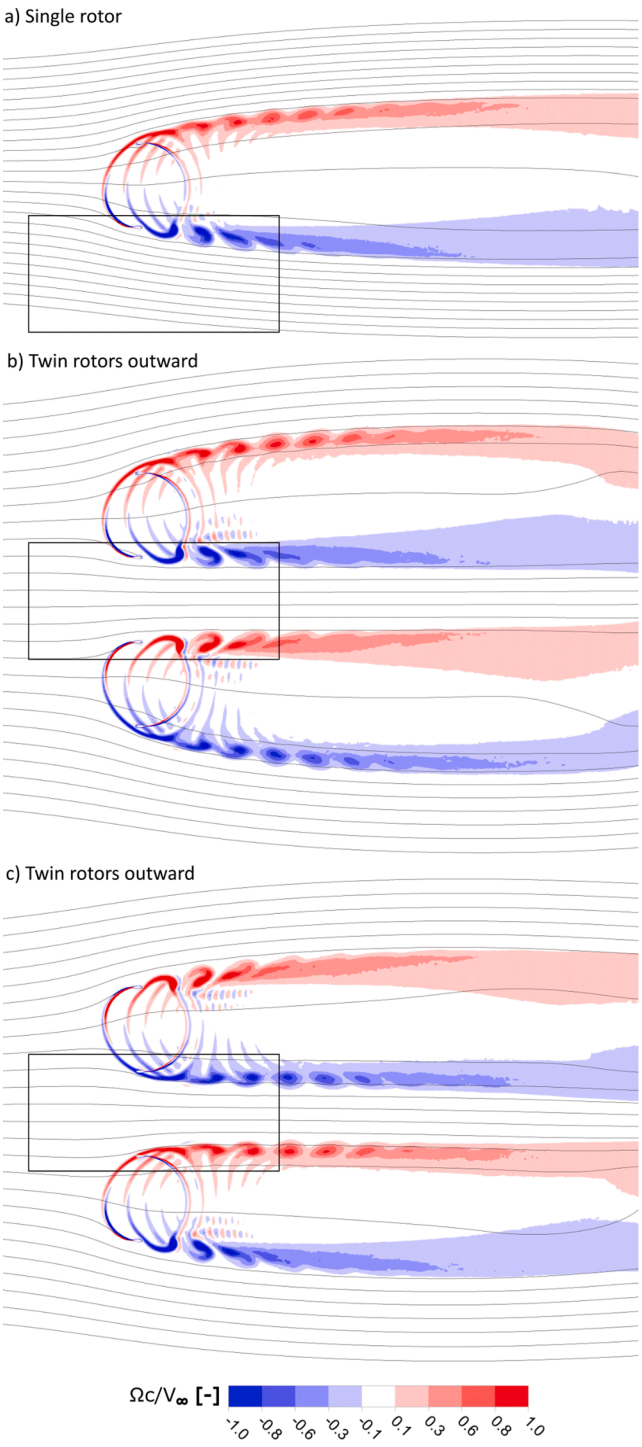

Fig. 11. DIMENSIONLESS contours and streamlines at TSR = 3 for a) single rotor, b) inward and c) outward twin rotors.

As a first step, it has been observed that the optimum operating point of twin rotors tends to increase to higher TSRs, in line with what was observed by Zanforlin et al. [15], Guilbot et al. [17], and Peng et al. [18]. The power augmentation mechanism was found to be the same at both TSR = 2.5 and TSR = 3, but the shift in the optimum operating conditions can be attributed to the more stable performance, resulting in a smoother variation of AoA, especially at the end of the first pitching-down phase and the beginning of the second pitching-up phase (i.e., $135^\circ < \theta < 225^\circ$ as shown in Fig. 10a). The quantitative analyses of the present study showed that this is mainly due to the higher blockage effect experienced by the twin rotors at higher rotational speed, resulting in producing a more consistent increase in the lift coefficient, as illustrated in Fig. 12, where the inward configuration at TSR 2.5 showed a continuous increase up to $\theta \approx 160^\circ$.

With respect to previous studies, the present one employed flow field sampling to extract the real angle of attack (AoA) and compute the effective lift and drag coefficients of the blade. The results revealed two key effects that arise due to the close deployment of turbines. First, the decrease in the axial induction factor indicated an increase in the momentum entering the turbine domain. This finding aligns with Alexander et al.'s [16] observation, as they suggested this effect to be the main source of power augmentation. However, differently from that study, it was found that the azimuth positions where the induction factor decreases are not always the same positions with enhanced efficiency. Secondly, the suppression of the cross-stream velocity component resulted in a reorientation of the relative velocity component, which was found to significantly enhance the lift generated by the blades. This latter finding, which Zanforlin et al. [15] identified as the main source of power increase, was quantified in this study to gain a better understanding of the power augmentation mechanism of twin rotors.

The results of the present work suggest that the power augmentation mechanism of the twin rotors follows a specific sequence. Firstly, the presence of two rotors generates a blockage effect in the mutual interaction zone. As a result, the stream tube expansion is eliminated, suppressing the cross-stream velocity component. Secondly, the straightening of the inflow increases the angle of attack (AoA) within the mutual interaction area, which increases the lift. Indeed, the change in the direction of the relative velocity also makes it become more oriented towards generating higher tangential forces. This is due to the fact that the lift component, which has now been reoriented to align with the increased AoA, is now also more aligned with the tangential force component. As a result, the mechanism is capable of enhancing both the lift and tangential force components, ultimately leading to an overall increase in power output. These effects are more pronounced for the inward configuration because the mutual interaction region lies in the area where most of the power generation takes place.

It is important to note that, based on the results presented in this paper, the power augmentation mechanism is mainly driven by the AoA increase. In fact, the latter observation could be useful in the design optimization of closely spaced Darrieus rotors starting from the airfoil selection up to the implementation of further power augmentation techniques, i.e., pitch control [27] and adding flow deflectors [14]. The findings could also be useful in validating and tuning low-fidelity models for closely spaced Darrieus turbines such as those in Refs. [6,8]. Future studies will be devoted at further investigating these aspects.

6. Conclusions

The flow physics around a pair of hydrokinetic Darrieus turbines have been investigated using two-dimensional CFD and a method to extrapolate the angle of attack from the solved flow field. This second method represented the key enabler to understand the impact of flow modifications at the blade level.

First, different spacings between the rotors have been investigated for both the *inward* and *outward* configurations: 1.8D, 2D, and 2.5D. The optimum spacing was found to be 2D for both *inward* and *outward* setups. With this spacing, the maximum power coefficient is however reached at different tip-speed ratios. Overall, it can be noted that the twin rotors operate at an optimum TSR higher than that of the single rotor. More specifically, the single rotor optimum TSR is 2.5, which corresponds to a C_P of 0.4. On the other hand, the *inward* setup showed the highest C_P of 0.46 at TSR = 3, while the *outward* setup had a maximum C_P of 0.43 at TSR = 2.75, with improvements of 16.1% and 8.7%, respectively.

Detailed results of the blade local flow field at both TSRs 2.5 and 3 showed an increase in the AoA within the area of mutual flow

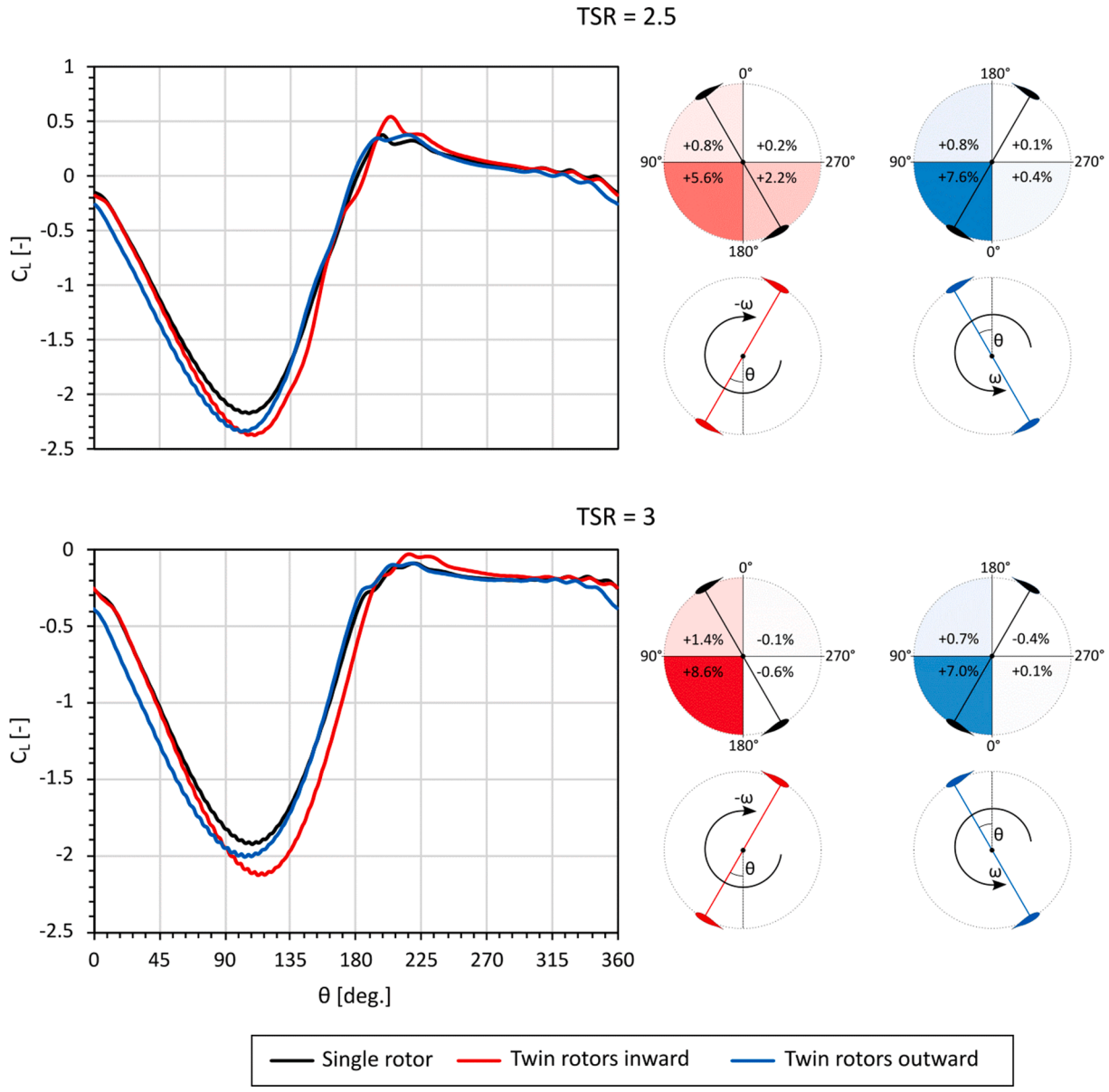

Fig. 12. Lift coefficient results on a single blade against azimuth position of a) inward b) outward configurations at S = 2D compared with that of the single rotor for one revolution.

interactions between the two adjacent rotors. It can be concluded that the blockage resulting from the flow field of the two closely spaced rotors forces the inflow to be straightened and suppresses the stream tube expansion effect. Thus, it causes a change in the relative velocity direction, which increases the AoA. This increase in the AoA allows the blade to generate higher lift compared to the single rotor. In the *inward* configuration, the blade experiences this increase in the AoA during the pitch-down phase, producing more lift than that of the isolated rotor. On the other hand, for the outward configuration, the blade experiences this AoA increase during the pitch-up phase, which causes a slight but not insignificant increase in the lift compared to the isolated rotor.

The following points summarize the main findings of this work:

- Deploying Darrieus rotors closely in an inline layout creates a blockage in the area between the rotors, forcing the inflow to be straightened, and eliminating the streamtube expansion effect between the rotors;
- The elimination of the streamtube expansion allows more momentum flux to enter the rotor domain. This effect has been quantified by computing the induction factor using the sampled flow field, showing that it has no direct relation with the increase in power coefficient;
- The change in the inflow direction creates a favorable increase in the AoA, which causes an increase in the lift force. The instantaneous lift coefficient has been computed in this work and is thought to be the main source of performance enhancement;
- The latter effects are more pronounced at higher rotational speeds. Therefore, the optimum power coefficient tends to shift towards higher TSRs in both the *inward* and *outward* setups;
- At TSR = 3, the lift generation increased by 8.6% in the second quarter of the *inward* setup, which corresponds to a 25.5% relative increase in the power coefficient. For the *outward* setup, it increased by 7% in the first quarter which corresponds to 18.8% in the power coefficient;
- The azimuth shift between the two adjacent rotors does not have any significant influence on effects leading to performance enhancement.

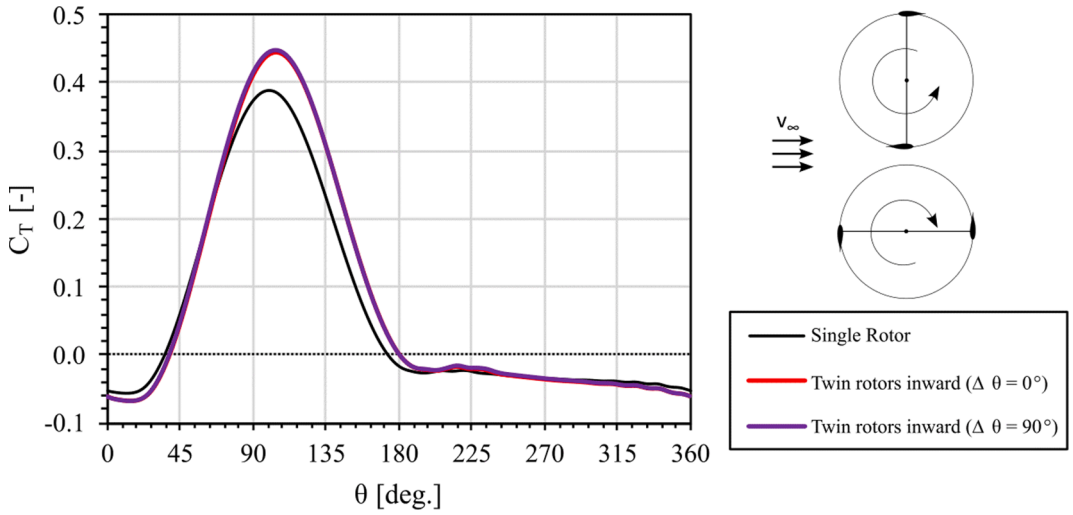

Fig. 13. Instantaneous torque coefficient variation against azimuth position for two twin rotors cases with different blade azimuth shifts, $\Delta\theta = 0^\circ$ and 90°, compared with that of the single rotor.

CRediT authorship contribution statement

Omar S. Mohamed: Conceptualization, Methodology, Software, Validation, Formal analysis, Investigation, Data curation, Writing – original draft, Visualization. **Pier Francesco Melani:** Methodology, Data curation, Writing – review & editing. **Francesco Balduzzi:** Conceptualization, Methodology, Writing – review & editing. **Giovanni Ferrara:** Supervision, Resources. **Alessandro Bianchini:** Conceptualization, Methodology, Investigation, Data curation, Writing – review & editing, Supervision, Project administration, Funding acquisition.

Declaration of Competing Interest

The authors declare that they have no known competing financial interests or personal relationships that could have appeared to influence the work reported in this paper.

Data availability

No data was used for the research described in the article.

References

[1] Kumar R, Raahemifar K, Fung AS. A critical review of vertical axis wind turbines for urban applications. Renew Sustain Energy Rev Jun. 2018;89:281–91. https://doi.org/10.1016/j.rser.2018.03.033.
[2] Paulsen US, Madsen HA, Hattel JH, Baran I, Nielsen PH. Design optimization of a 5 MW floating offshore vertical-axis wind turbine. Energy Procedia Jan. 2013;35:22–32. https://doi.org/10.1016/j.egypro.2013.07.155.
[3] Tjiu W, Marnoto T, Mat S, Ruslan MH, Sopian K. Darrieus vertical axis wind turbine for power generation II: challenges in HAWT and the opportunity of multi-megawatt Darrieus VAWT development. Renew Energy Mar. 2015;75:560–71. https://doi.org/10.1016/j.renene.2014.10.039.
[4] Fadil J, Soedibyo, Ashari M, Performance comparison of vertical axis and horizontal axis wind turbines to get optimum power output. In: 2017 15th International Conference on Quality in Research (QiR): International Symposium on Electrical and Computer Engineering, Jul. 2017. p. 429–33. doi: 10.1109/QIR.2017.8168524.
[5] Dabiri JO. Potential order-of-magnitude enhancement of wind farm power density via counter-rotating vertical-axis wind turbine arrays. J Renew Sustain Energy Jul. 2011;3(4):043104. https://doi.org/10.1063/1.3608170.
[6] Vergaerde A, De Troyer T, Standaert L, Kluczewska-Bordier J, Pitance D, Immas A, et al. Experimental validation of the power enhancement of a pair of vertical-axis wind turbines. Renew Energy 2020;146:181–7.
[7] Parneix N, Fuchs R, Immas A, Silvert F, Efficiency improvement of vertical-axis wind turbines with counter-rotating lay-out. In: Proceedings of EWEA 2016.
[8] Cacciali L, Battisti L, Dell'Anna S. Multi-array design for hydrokinetic turbines in hydropower canals. Energies Jan. 2023;16:5. https://doi.org/10.3390/en16052279.
[9] Li S, Li Ye, Yang C, Wang Q, Zhao B, Li D, et al. Experimental investigation of solidity and other characteristics on dual vertical axis wind turbines in an urban environment. Energ Conver Manage 2021;229:113689. https://doi.org/10.1016/j.enconman.2020.113689.
[10] Müller S, Muhawenimana V, Wilson CAME, Ouro P. Experimental investigation of the wake characteristics behind twin vertical axis turbines. Energ Conver Manage Nov. 2021;247:114768. https://doi.org/10.1016/j.enconman.2021.114768.
[11] Mohamed OS, Ibrahim A, El Baz AMR. CFD Investigation of the multiple rotors Darrieus type turbine performance.In: Presented at the ASME Turbo Expo 2019: Turbomachinery Technical Conference and Exposition, Nov. 2019. doi: 10.1115/GT2019-91491.
[12] Zheng H-D, Zheng XY, Zhao SX. Arrangement of clustered straight-bladed wind turbines. Energy Jun. 2020;200:117563. https://doi.org/10.1016/j.energy.2020.117563.
[13] Sahebzadeh S, Rezaeiha A, Montazeri H. Towards optimal layout design of vertical-axis wind-turbine farms: double rotor arrangements. Energ Conver Manage Dec. 2020;226:113527. https://doi.org/10.1016/j.enconman.2020.113527.
[14] Zhao P, Jiang Y, Liu S, Stoesser T, Zou L, Wang K. Investigation of fundamental mechanism leading to the performance improvement of vertical axis wind turbines by deflector. Energ Conver Manage Nov. 2021;247:114680. https://doi.org/10.1016/j.enconman.2021.114680.
[15] Zanforlin S, Nishino T. Fluid dynamic mechanisms of enhanced power generation by closely spaced vertical axis wind turbines. Renew Energy Dec. 2016;99:1213–26. https://doi.org/10.1016/j.renene.2016.08.015.
[16] Alexander AS, Santhanakrishnan A. Mechanisms of power augmentation in two side-by-side vertical axis wind turbines. Renew Energy Apr. 2020;148:600–10. https://doi.org/10.1016/j.renene.2019.10.149.
[17] Guilbot M, Barre S, Balarac G, Bonamy C, Guillaud N. A numerical study of Vertical Axis Wind Turbine performances in twin-rotor configurations. J Phys: Conf Ser Sep. 2020;1618(5):052012. https://doi.org/10.1088/1742-6596/1618/5/052012.
[18] Peng HY, Han ZD, Liu HJ, Lin K, Lam HF. Assessment and optimization of the power performance of twin vertical axis wind turbines via numerical simulations. Renew Energy Mar. 2020;147:43–54. https://doi.org/10.1016/j.renene.2019.08.124.
[19] Miller MA, Duvvuri S, Hultmark M. Solidity effects on the performance of vertical-axis wind turbines. Flow 2021;1:E9. https://doi.org/10.1017/flo.2021.9.
[20] Rahimi H, Schepers JG, Shen WZ, García NR, Schneider MS, Micallef D, et al. Evaluation of different methods for determining the angle of attack on wind turbine blades with CFD results under axial inflow conditions. Renew Energy 2018;125:866–76.
[21] Bianchini A, Balduzzi F, Ferrara G, Persico G, Dossena V, Ferrari L. A critical analysis on low-order simulation models for darrieus vawts: how much do they pertain to the real flow? J Eng Gas Turbines Power Sep. 2018;141(1). https://doi.org/10.1115/1.4040851.
[22] Jost E, Klein L, Leipprand H, Lutz T, Krämer E. Extracting the angle of attack on rotor blades from CFD simulations. Wind Energy 2018;21(10):807–22. https://doi.org/10.1002/we.2196.
[23] Elsakka MM, Ingham DB, Ma L, Pourkashanian M. CFD analysis of the angle of attack for a vertical axis wind turbine blade. Energ Conver Manage Feb. 2019;182:154–65. https://doi.org/10.1016/j.enconman.2018.12.054.
[24] Melani PF, Balduzzi F, Ferrara G, Bianchini A. How to extract the angle attack on airfoils in cycloidal motion from a flow field solved with computational fluid dynamics? Development and verification of a robust computational procedure. Energ Conver Manage Nov. 2020;223:113284. https://doi.org/10.1016/j.enconman.2020.113284.
[25] Mohamed OS, Elbaz AMR, Bianchini A. A better insight on physics involved in the self-starting of a straight-blade Darrieus wind turbine by means of two-dimensional

Computational Fluid Dynamics. J Wind Eng Ind Aerodyn Nov. 2021;218:104793. https://doi.org/10.1016/j.jweia.2021.104793.
[26] Balduzzi F, Melani PF, Soraperra G, Brighenti A, Battisti L, Bianchini A. Some design guidelines to adapt a Darrieus vertical axis turbine for use in hydrokinetic applications. E3S Web Conf 2021;312:08017. https://doi.org/10.1051/e3sconf/202131208017.
[27] Melani PF, Balduzzi F, Ferrara G, Bianchini A. Development of a desmodromic variable pitch system for hydrokinetic turbines. Energ Conver Manage Dec. 2021;250:114890. https://doi.org/10.1016/j.enconman.2021.114890.
[28] Melani PF, Balduzzi F, Ferrara G, Bianchini A. Tailoring the actuator line theory to the simulation of Vertical-Axis Wind Turbines. Energ Conver Manage Sep. 2021;243:114422. https://doi.org/10.1016/j.enconman.2021.114422.
[29] Mohamed OS, Melani PF, Balduzzi F, Ferrara G, Bianchini A. An insight on the key factors influencing the accuracy of the actuator line method for use in vertical-axis turbines: Limitations and open challenges. Energ Conver Manage Oct. 2022;270:116249. https://doi.org/10.1016/j.enconman.2022.116249.
[30] Two-equation eddy-viscosity turbulence models for engineering applications | AIAA Journal. https://arc.aiaa.org/doi/abs/10.2514/3.12149?journalCode=aiaaj (accessed Nov. 13, 2022).
[31] Balduzzi F, Bianchini A, Maleci R, Ferrara G, Ferrari L. Critical issues in the CFD simulation of Darrieus wind turbines. Renew Energy Jan. 2016;85:419–35. https://doi.org/10.1016/j.renene.2015.06.048.
[32] Campobasso MS, Yan M, Bonfiglioli A, Gigante FA, Ferrari L, Balduzzi F, et al. Low-speed preconditioning for strongly coupled integration of Reynolds-averaged Navier-Stokes equations and two-equation turbulence models. Aerosp Sci Technol 2018;77:286–98.
[33] Ibrahim AA, Elbaz AMR, Melani PF, Mohamed OS, Bianchini A. Power augmentation of Darrieus wind turbine blades using trapped vortex cavity. J Wind Eng Ind Aerodyn Apr. 2022;223:104949. https://doi.org/10.1016/j.jweia.2022.104949.
[34] Balduzzi F, Bianchini A, Ferrara G, Ferrari L. Dimensionless numbers for the assessment of mesh and timestep requirements in CFD simulations of Darrieus wind turbines. Energy Feb. 2016;97:246–61. https://doi.org/10.1016/j.energy.2015.12.111.
[35] Wang Y, Sun XJ, Zhu B, Zhang HJ, Huang DG. Effect of blade vortex interaction on performance of Darrieus-type cross flow marine current turbine. Renew Energy Feb. 2016;86:316–23. https://doi.org/10.1016/j.renene.2015.07.089.
[36] Drela M, XFOIL: An Analysis and design system for low reynolds number airfoils. In: Conference on Low Reynolds Number Airfoil Aerodynamics, University of Notre Dame, Jun. 1989. doi: 10.1007/978-3-642-84010-4_1.
[37] Rainbird JM, Bianchini A, Balduzzi F, Peiró J, Graham JMR, Ferrara G, et al. On the influence of virtual camber effect on airfoil polars for use in simulations of Darrieus wind turbines. Energ Conver Manage 2015;106:373–84.
[39] Bianchini A, Balduzzi F, Bachant P, Ferrara G, Ferrari L. Effectiveness of two-dimensional CFD simulations for Darrieus VAWTs: a combined numerical and experimental assessment. Energ Conver Manage Mar. 2017;136:318–28. https://doi.org/10.1016/j.enconman.2017.01.026.
[40] Rezaeiha A, Montazeri H, Blocken B. On the accuracy of turbulence models for CFD simulations of vertical axis wind turbines. Energy Aug. 2019;180:838–57. https://doi.org/10.1016/j.energy.2019.05.053.
[41] Syawitri TP, Yao YF, Chandra B, Yao J. Comparison study of URANS and hybrid RANS-LES models on predicting vertical axis wind turbine performance at low, medium and high tip speed ratio ranges. Renew Energy May 2021;168:247–69. https://doi.org/10.1016/j.renene.2020.12.045.
[42] Rezaeiha A, Montazeri H, Blocken B. Towards accurate CFD simulations of vertical axis wind turbines at different tip speed ratios and solidities: Guidelines for azimuthal increment, domain size and convergence. Energ Conver Manage Jan. 2018;156:301–16. https://doi.org/10.1016/j.enconman.2017.11.026.
[43] Balduzzi F, Drofelnik J, Bianchini A, Ferrara G, Ferrari L, Campobasso MS. Darrieus wind turbine blade unsteady aerodynamics: a three-dimensional Navier-Stokes CFD assessment. Energy Jun. 2017;128:550–63. https://doi.org/10.1016/j.energy.2017.04.017.
[44] Nazari S, Zamani M, Moshizi SA. Comparison between two-dimensional and three-dimensional computational fluid dynamics techniques for two straight-bladed vertical-axis wind turbines in inline arrangement. Wind Engineering. Dec 2018;42:647–64. https://doi.org/10.1177/0309524X18780384.

Further reading

[38] Jin G, Zong Z, Jiang Y, Zou L. Aerodynamic analysis of side-by-side placed twin vertical-axis wind turbines. Ocean Eng Aug. 2020;209:107296. https://doi.org/10.1016/j.oceaneng.2020.107296.